J. Micromech. Microeng. **20** (2010) 035020 (9pp) doi:10.1088/0960-1317/20/3/035020

Microscale-modulated porous coatings: fabrication and pool-boiling heat transfer performance

Ömer Necati Cora[1], **Dahye Min**[2], **Muammer Koç**[1,3] **and Massoud Kaviany**[2]

[1] NSF IUCRC-Center for Precision Forming (CPF), Virginia Commonwealth University (VCU), Richmond, VA, USA
[2] Department of Mechanical Engineering, University of Michigan, Ann Arbor, MI 48109-2125, USA

E-mail: mkoc@vcu.edu

Received 24 November 2009, in final form 4 January 2010
Published 15 February 2010
Online at stacks.iop.org/JMM/20/035020

Abstract
The manufacture of microscale-modulated coatings (periodic, porous stacks with a thin base layer) under mass-production conditions was investigated experimentally to establish robust process parameters. Copper powders (average diameter of 100 μm) were compacted on a copper substrate under controlled pressure, temperature, surface geometry and processing sequences (e.g., sintering before and after compaction). Porosity, stack height, pitch and base thickness of coatings were measured. Results show that a minimum temperature of 350 °C and pressure of 25 MPa are required for permeable coatings, when sintering is carried out after compaction. When 'sintering before compaction' is followed, pressure values in excess of 100 MPa are needed and surfaces from this approach block the pores and diminish permeability. Pool boiling heat transfer experiments were conducted on selected coatings, showing that the best enhancement is by low-pressure compation coatings.

1. Introduction

Microscale porous and modulated surface coatings have been shown to offer enhanced heat transfer efficiencies [1–10]. Various fabrication methods to achieve such surfaces were considered and experimented with as published in previous studies [11–17]. Warm powder compaction is considered to be a promising option to ensure microscale-modulated surfaces with controllable porosity at low cost and high production rates [16]. Furthermore, it was also proven to ensure necessary bonding of powders to thin substrates in a single action operation [17]. Nevertheless, achieving a controlled porosity and a strong bonding between powders and a substrate needs to be compromised at an optimal level since increased compaction pressure is essential for bonding the powders to the substrate, whereas high porosity requires minimal levels of the same.

This study, which is based on previous findings as reported in [17–19], is aimed at determining appropriate processing parameters (pressure, temperature, geometry) and sequences (sintering before or after compaction) for robust, cost-effective mass manufacturing of microscale, porous and modulated surface structures. Two sets of design of experiment (DOE) studies were conducted using the experimental setup and methodology as desribed in detail in [18]. Selected modulated porous surface samples were then tested under pool boiling conditions, as explained in [19], to determine their superheat behavior and critical heat flux (CHF) and to compare with other surface coatings. In the next section, micro-manufacturing experiments, experimental conditions and methodology are presented. In section 3, micro-manufacturing experiment results are discussed in detail. Pool boiling experiments and results are explained in section 4. In the final section, conclusions are summarized followed by a list of recommended future work.

[3] Author to whom any correspondence should be addressed.

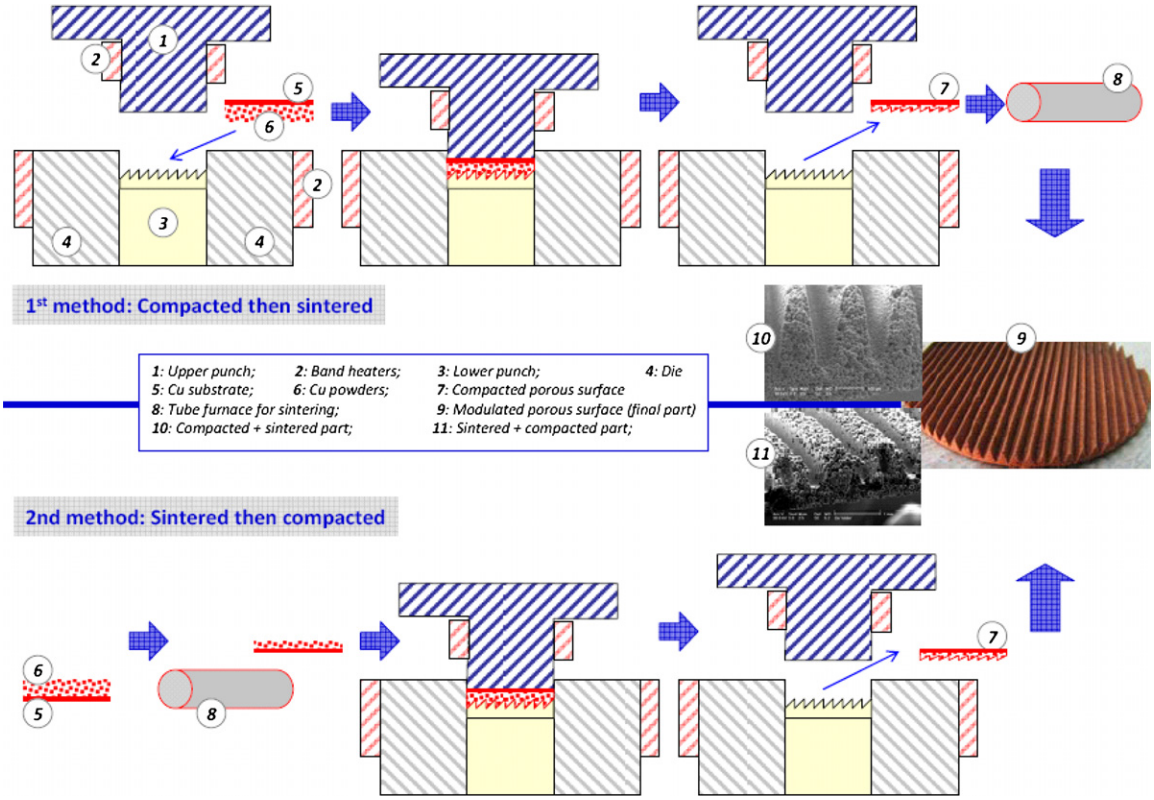

Figure 1. Experimental procedure for both methods.

2. Micro-manufacturing experiments, conditions and method

For a detailed description of the experimental setup used in this study, readers are referred to a previous publication [18]. Based on experience and knowledge gained through previous studies [17–19], two sets of DOE studies were conducted to investigate the effect of processing sequence as depicted in figure 1. In the first set (first method), copper powders of 100 μm average size were first warm compacted and then sintered at around 900 °C. In the second set (second method), similar powders were first sintered and then compacted at different temperature and pressure levels to generate micro-channels. Each test was repeated at least three times. In all experiments, sieved Cu powders approximately, 100 μm in diameter from 'A' Spherical Copper Powder Grade 61 were used [20]. About 90% of the powders were in the range of 80–110 μm in diameter after the sieving process.

During the experiments where the first method procedures were followed (figure 1), at the beginning of each experiment, the lower die (punch with grooves/channels) was placed 0.7 mm lower than the container's upper surface to create a cavity. This cavity was filled with copper powders. A thin copper substrate of 0.4 mm thickness was placed on top of the poured powders. Then, the upper die was inserted against the thin substrate. Heating of the entire die set was achieved through band heaters around the upper and lower dies. Two thermocouples were used to measure and record the temperature on the dies. The selection of the thermocouple placement was determined via finite element heat transfer analysis. Once both upper and lower dies/punch reached the desired temperature level (350, 425 or 500 °C), the upper die was moved down in a controlled manner by the Instron machine's load/displacement control systems to the desired level of pressure. After compaction tests, specimens were taken out of the die and sintered at a temperature of 900 °C for 1 h under a controlled atmosphere in a tube furnace (OTF-1200Y Quartz Tube Furnace, MTI Corp., CA, USA). Based on the minimum and maximum P and T values from the preliminary tests, and the three different surface geometry conditions, a DOE matrix was established and a Box–Behnken type 'response surface design' was selected to minimize the number of experiments using MINITAB software [21]. Surface geometry (*Aspect Ratio*, AR (h/w: *height/width of an individual feature*), $AR_1 = 0$, $AR_2 = 0.84$, $AR_3 = 1.68$), pressure ($P_1 = 15$, $P_2 = 32.5$, $P_3 = 50$ MPa) and temperature ($T_1 = 350$, $T_2 = 425$, $T_3 = 500$ °C) were used as experimental factors. The porosity level (%) and the thickness at the valley (t_v) were identified as the response parameters. In order to accurately assess the effect of experimental parameters on the variation of the responses, each experiment was repeated three times. Consequently, a total of 42 experiments were performed. Optical microscope and SEM pictures of the compacted samples are shown in figure 2. Table 1 shows the full DOE matrix for the first set of experiments and the measurement results for porosity and valley thickness values. Likewise, figure 3 depicts the corresponding porosity and valley thickness measurements.

Table 1. Full DOE chart for experiments following the first methodology.

Run order	Pressure (MPa)	Temperature (°C)	Geometry/ aspect ratio	Porosity (%)	Valley thickness (μm)
1	15	425	Flat/0	30	1278.0
18	15	425	Flat/0	29	1315.6
38	15	425	Flat/0	31	1270.0
5	32.5	350	Flat/0	20	1265.3
15	32.5	350	Flat/0	21	1250.0
29	32.5	350	Flat/0	23	1288.0
3	32.5	500	Flat/0	19	1207.8
22	32.5	500	Flat/0	18	1225.0
33	32.5	500	Flat/0	19	1260.0
4	50	425	Flat/0	15	1197.5
20	50	425	Flat/0	17	1210.0
34	50	425	Flat/0	18	1182.0
8	15	350	Large feature/0.84	35	345.0
27	15	350	Large feature/0.84	33	395.0
41	15	350	Large feature/0.84	34	410.0
14	15	500	Large feature/0.84	30	322.0
17	15	500	Large feature/0.84	31	368.0
40	15	500	Large feature/0.84	32	318.0
7	32.5	425	Large feature/0.84	29	245.0
11	32.5	425	Large feature/0.84	27	225.2
19	32.5	425	Large feature/0.84	27	261.4
28	32.5	425	Large feature/0.84	31	272.0
31	32.5	425	Large feature/0.84	35	280.0
39	32.5	425	Large feature/0.84	29	260.0
6	50	350	Large feature/0.84	25	265.0
23	50	350	Large feature/0.84	23	276.3
37	50	350	Large feature/0.84	25	283.0
10	50	500	Large feature/0.84	20	291.2
25	50	500	Large feature/0.84	21	211.1
32	50	500	Large feature/0.84	27	158.8
9	15	425	Small feature/1.68	32	226.0
21	15	425	Small feature/1.68	28	198.0
35	15	425	Small feature/1.68	29	191.0
2	32.5	350	Small feature/1.68	25	129.0
16	32.5	350	Small feature/1.68	26	132.0
42	32.5	350	Small feature/1.68	25	128.0
12	32.5	500	Small feature/1.68	24	126.0
26	32.5	500	Small feature/1.68	25	134.0
30	32.5	500	Small feature/1.68	25	138.0
13	50	425	Small feature/1.68	22	120.0
24	50	425	Small feature/1.68	24	125.0
36	50	425	Small feature/1.68	22	120.0

In the second set of experiments (as depicted in figure 1), copper powders of the same size and distribution were placed on a copper substrate of similar thickness and grade in a ceramic mold to control the height of the poured powders. Then, several of them were placed in the tube furnace for sintering, resulting in a 0.7 mm thick porous layer on the solid substrate. After sintering, these samples were compacted in the same experimental setup as before but under different pressure and temperature conditions. Based on the findings of heat transfer tests for the first set of experiments which will be discussed in section 4, only the surface geometry with small micro-channels with an aspect ratio AR of 1.68 was experimented with. The purpose of this set of experiments was to understand if sintered or sprayed surfaces could effectively be compacted into modulated surface structures that would facilitate automation and cost-effective mass production conditions. After some trial experiments, it was observed that the strength level of the surfaces increased. Hence, relatively higher pressure levels, namely 75, 100 and 125 MPa, with lower temperature levels of 100, 150 and 200 °C were used in this set of experiments as tabulated in table 2. The porosity and valley thickness measurements are also shown in table 2.

3. Experimental results and discussion

3.1. Porosity measurements and analysis for experiments with the first method

The compacted and sintered specimens were cut into four pieces for porosity and dimensional measurement and analyses. A further description of measurement methods can be found in [18]. Figure 4(*a*) illustrates the response surface plots for porosity as a function of pressure and temperature (top figure) and temperature and geometry (bottom figure), while

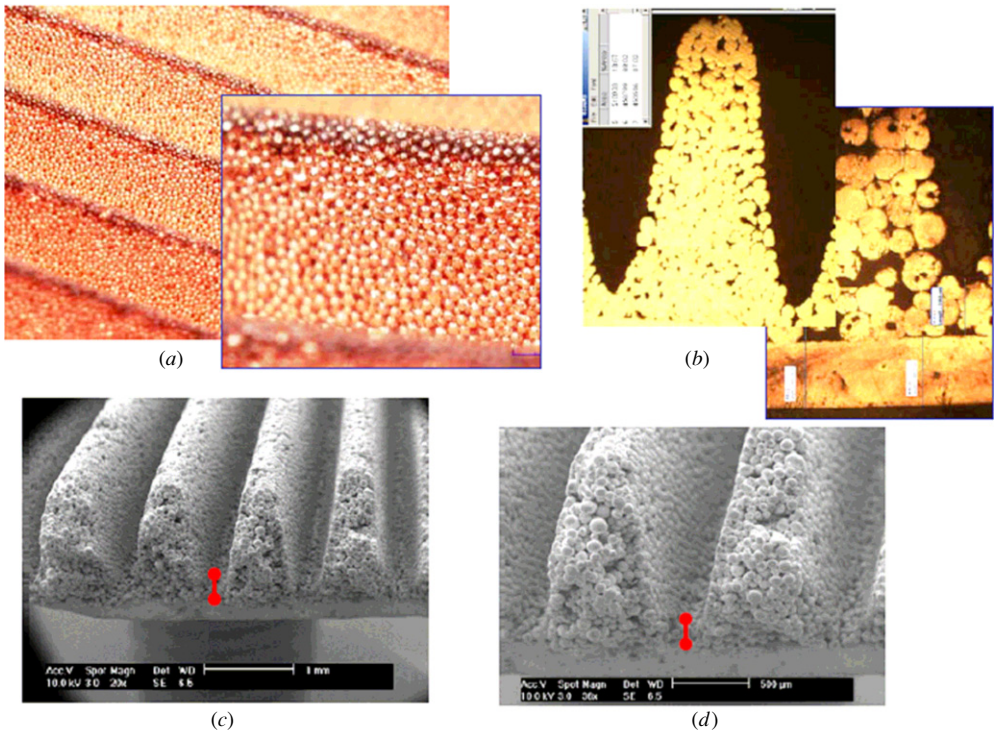

Figure 2. (*a*) Optical microscope pictures of the powder compacted channels with 50× and 100× magnification (provided by HIROX-USA Inc., NJ, USA using a KH-7700 digital microscope); (*b*) micrographs of single channels used for image analysis to measure porosity and valley thickness; SEM of sample 309 at a magnification factor of (*c*) 20×; (*d*) 36×.

Table 2. DOE chart for experiments following the second method using only the surface geometry with AR of 1.68 (small channels).

Run order	Pressure (MPa)	Temperature (°C)	Porosity (%)	Valley thickness (μm)
5	75	100	35	541.7
9	75	100	38	674.2
1	75	100	37	1002.5
3	75	150	36	743.4
11	75	200	41	1090.1
7	75	200	40	568.2
6	100	100	41	694.2
13	100	150	34	823.6
14	100	150	31	625.7
15	100	150	33	629.6
10	125	100	39	693.0
2	125	100	35	681.7
4	125	200	36	386.7
8	125	200	30	750.2
12	125	200	31	532.6

figure 4(*b*) depicts the dispersion of experimental data for porosity as a function of the same parameters. The important conclusions from this figure are: (1) the effect of temperature is not as significant as that of pressure and (2) the effect of geometry difference on the porosity level for the two types of modulated surfaces (AR = 0.84, AR = 1.68) is insignificant, though slightly higher porosity levels can be attained with large channels (i.e. AR = 0.84). As a result, for mass production and high heat transfer efficiency concerns: (1) the temperature level can be kept lower to save energy and cost, (2) the selection and control of pressure should be performed based on the surface geometry and (3) the size of the modulations (i.e. smaller versus larger channels) should be decided based on heat transfer efficiency, as will be discussed in section 4.

3.2. Valley thickness measurements and analysis

The valley thickness, t_v, is defined as the distance between the top surface of the substrate and the lowest point of the channel. It was stated by Litter and Kaviany that the optimal value of this parameter is one to two particle diameters (d) in order to minimize the surface superheat (or the wick thermal resistance) [5]. Beyond this level, the heat transfer efficiency of the modulated surfaces drops to the same degree of a uniform surface layer. In this study, valley thickness values of surfaces were measured using the optical microscopy images at different cross-sections and locations on the specimen as depicted in figure 2. From ANOVA analyses, the effects of temperature and pressure on the valley thickness were found to be less significant compared to the effect of geometry as can be seen in figure 5(*a*). Figure 5(*b*) illustrates the data points for valley thickness measurements for all samples with respect to geometry and pressure (top figure), geometry and temperature (bottom figure). Although the AR seemed to be a significant factor affecting the valley thickness as depicted in figures 5(*a*) and (*b*), it should be noted that the AR = −1 refers to the 'flat surface type' samples that are different from other channeled types of samples. The change in the valley thicknesses between the two different channeled surfaces (AR 0.84 and 1.68) is negligible.

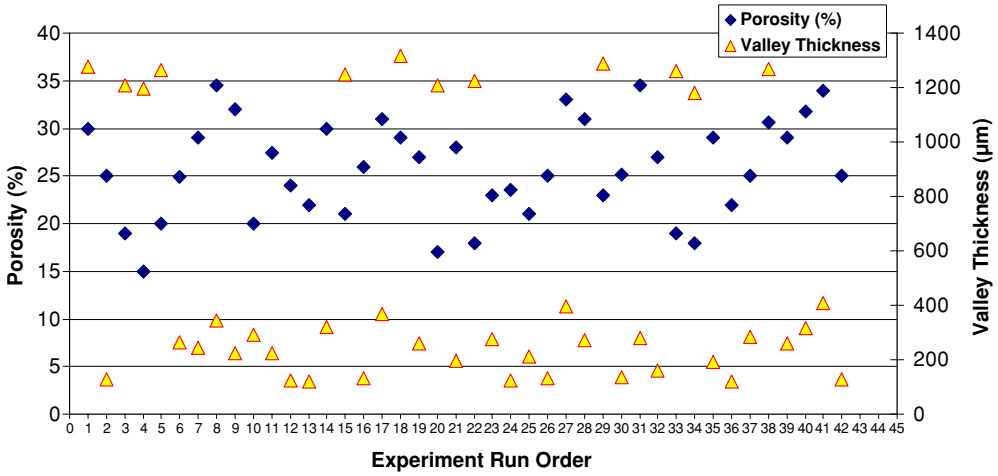

Figure 3. Corresponding porosity and valley thickness measurements for all the samples produced with the first method.

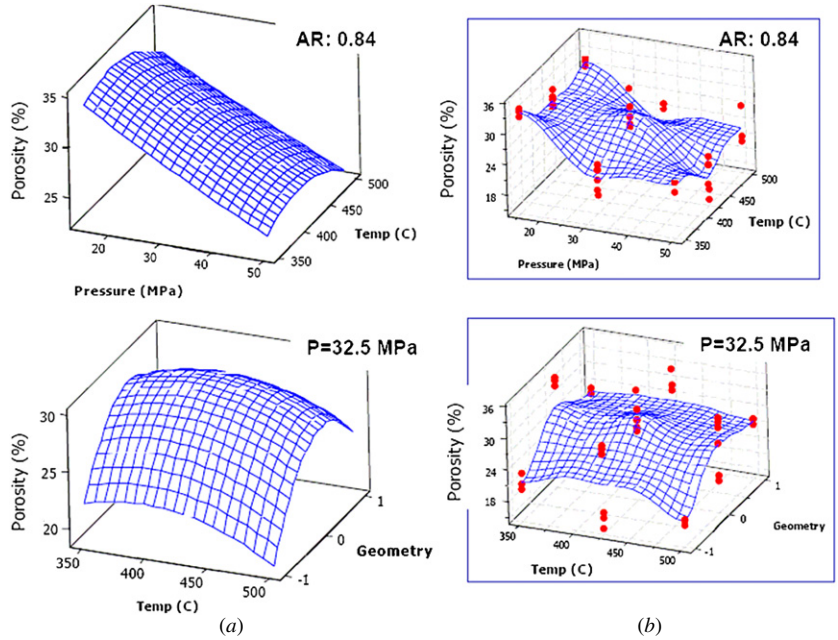

(*a*) (*b*)

Figure 4. (*a*) Response surface (estimation) plots and (*b*) data points for porosity measurement obtained for samples produced with the first method as a function of pressure, temperature and geometry, (−1: aspect ratio = 0; 0: AR = 0.84; 1: AR = 1.68). ANOVA response surface regression result for porosity (including insignificant terms): porosity (%) = $-14.4778 - 0.4211(P) + 0.2738(T) - 0.0003(T^2) - 5.2048(\mathrm{AR}^2) + 0.0866(P)(\mathrm{AR})$. Reduced ANOVA response surface regression result for porosity (after dropping the insignificant terms): porosity (%) = $-14.4778 - 0.4211(P) + 0.2738(T) - 5.2048(\mathrm{AR}^2)$, R^2 (correlation): 92%.

3.3. Porosity and valley thickness analyses for experiments with the second method

Porosity and valley thickness measurements for the samples, which were sintered prior to compaction process, were obtained with the same procedure as mentioned in section 3.1. Figure 6 shows the SEM and micrograph pictures of porous surfaces obtained by the second method at different magnification levels. The effects of pressure and temperature on porosity and valley thickness are shown in figure 7. Figure 7(*a*) illustrates the dispersion of measured data points for porosity, while figure 7(*b*) depicts the experimental measurements for valley thickness, both as a function of pressure and temperature. Contrary to the experimental results with the first method, temperature has a considerable effect on the porosity in the second set of experiments. Figure 7 shows that the porosity level has a tendency to reach low values at about 150 °C with increasing pressure, while relatively high porosity values were obtained at peak temperatures (100 and 200 °C). Valley thickness values decrease with increasing pressure as expected since better channel formation is obtained. The highest valley thickness values were obtained under high temperature–low pressure conditions while the lowest valley thickness values were obtained at high pressure–high temperature conditions as depicted in figure 7(*a*). It can be seen that relatively high porosity levels and valley

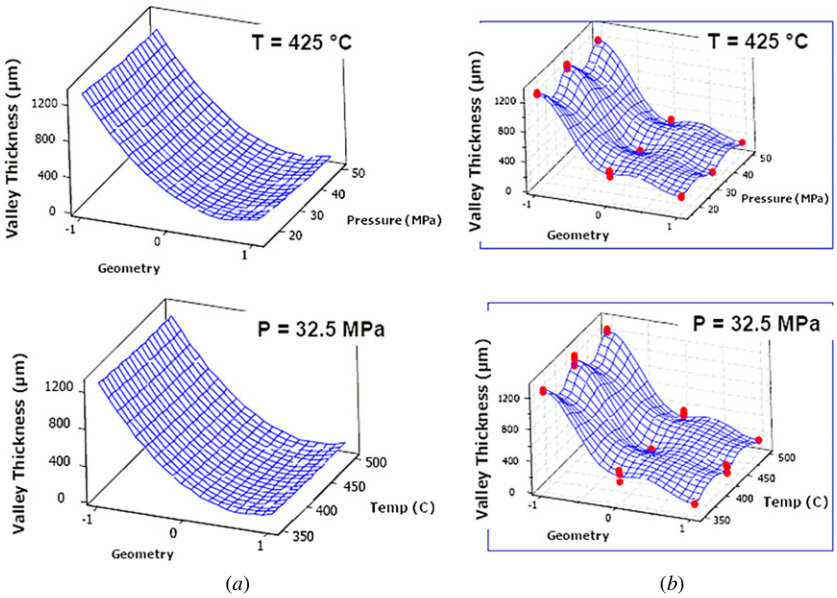

(*a*) (*b*)

Figure 5. (*a*) Response surface plots and (*b*) data points for valley thickness (t_v) as a function of compacting pressure, temperature and geometry (−1: aspect ratio = 0; 0: AR = 0.84; 1: AR = 1.68) for the samples obtained with the first method. ANOVA response surface regression result for valley thickness (including insignificant terms): Valley thickness (μm) = 1072.27 − 8.52(P) − 609.42(AR) + 0.10(P^2) +416.07(AR^2), R^2: 98%.

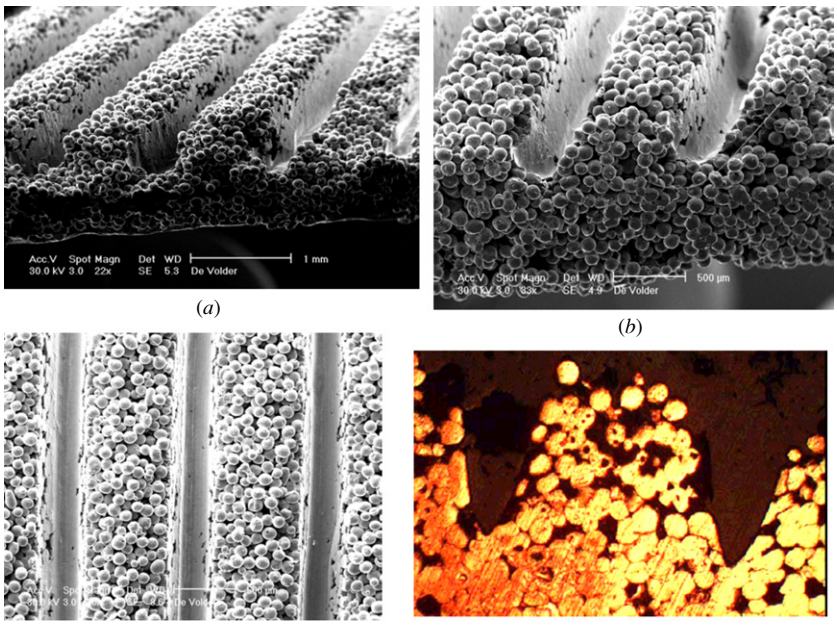

(*a*) (*b*) (*c*) (*d*)

Figure 6. SEM images of the surface manufactured by the second method at (*a*) 22×, (*b*) 33×, (*c*) 30× magnification, (*d*) micrograph picture used in porosity and valley thickness measurements.

thickness values were measured with the pre-sintered process when tables 1 and 2 are compared. This is mainly due to the increased yield strength of the powders by the pre-sintering process before the compaction was performed. Another significant outcome of the second method (i.e. pre-sintering before compaction) is the formation of incomplete channels as seen in figures 6(*a*)–(*c*). It is also observed that the deformation of individual powders was less compared to the first method, leading to weaker bonds between powders, and hence, to incomplete peaks. However, the powders on the lateral surfaces (side walls) of the channels were excessively deformed causing the closing of pores. These powders underwent high deformation and connected to each other because of the direct impingement of die channels on these surfaces with relatively high-pressure levels (125 MPa max in the second method and 50 MPa max with the first method). It is believed that the high-pressure levels overcame the friction between powders and resulted in the formation of a nonporous layer as seen in figure 6. The effect of this nonporous layer on heat transfer will be discussed in section 4.

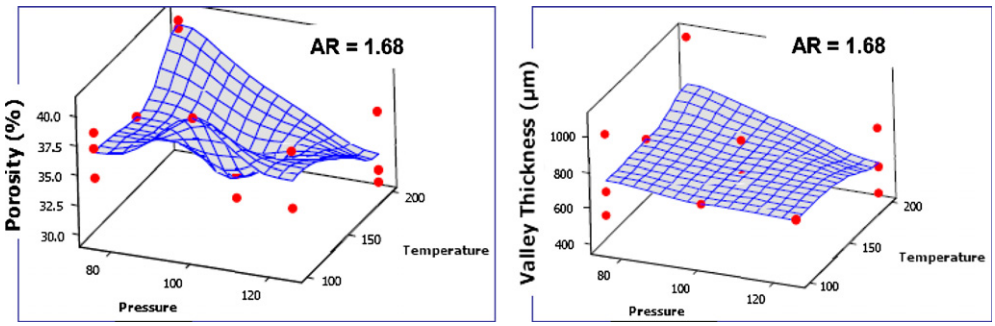

(*a*) (*b*)

Figure 7. Measurement data for (*a*) porosity, (*b*) valley thickness as a function of pressure, temperature and geometry for the samples produced with the second method.

4. Pool boiling experiments and results

Detailed information on Zuber hydrodynamic theory, nucleate boiling and critical heat flux as well as a description of the experimental procedure are reported in [5, 7] and the results for specimens fabricated by the first method are presented in [19].

4.1. Pool boiling experiments

Each specimen (a copper disk coated with modulated porous layer) is silver soldered to a cylindrical solid copper base of the same diameter and 4.5 cm height. Using high thermal conductivity paste, this is in turn attached to a large insulated copper thermal mass by clamping plates. The heat from two electrical heaters (1.0 and 1.3 kW) is applied to the lower half of the insulated thermal mass. As a working fluid, pentane is used at atmospheric pressure inside a Pyrex glass reservoir. Five E-type thermocouples are aligned in the axial direction along the copper test piece and the thermal mass. These recorded temperatures are used to evaluate the thermal conductivity of the copper and determine the heat flux through the test piece by the Fourier law of conduction. The saturation temperature of pentane $[T_{lg}(p_g)]$ is measured by a thermocouple located above the specimen, where p_g is vapor pressure. The surface temperature underneath the specimen (T_s) is determined by the extrapolation of measured temperature. The heat flux and the saturation temperature are calculated as averages over 2 min at the quasi-steady state, as the power is increased incrementally. The critical heat flux (q_{CHF}) is the last observed quasi-steady state just before a sudden temperature increase with a smallest rise in the power. The measured heat flux q and the surface superheat T_s–T_{lg}, up to q_{CHF}, are shown in figure 8.

An estimate of the uncertainties in the thermophysical property values is about 0.5%, in the thermocouples recording the surface superheat (temperature difference across the coating) about 0.5 °C, in the position measurement about 0.5 mm and in the heat flux including the critical flux about 5%. The percentage uncertainty in the heat flux measurement would increase with decreasing heat flux. All experiments are done at 1 atm pressure, so the saturation temperature matches this pressure. We have also measured temperature at various locations above the surface and it is the saturation temperature.

Table 3. Test conditions for the samples given in figure 6.

Surface no	Pressure (MPa)	Temperature (°C)	h/w (AR)	Porosity (%)	Powder size (μm)
302	32.5	350	Small/1.68	25	100
313	50	425	Small/1.68	22	100
143 [19]	25	350	Small/1.68	36	200
147 [19]	50	350	Large/0.84	27	200
150 [19]	50	350	Small/1.68	30	200

4.2. Results

The effects of coating attributes on q versus T_s–T_{lg} and q_{CHF} are recorded for the specimens fabricated by the first method and are shown in figure 8. This figure shows the measured q with respect to the wick superheat for specimens 143, 147, 150, 302 and 313 (first three samples are from authors' previous studies referenced in the text, and their compaction test conditions are given in table 3), as well as uniform coating and plain surfaces, for comparison of different channel widths.

The critical heat flux of $q_{\mathrm{CHF}} = 485$ kW m^{-2} for the uniform-coating surface with $d_p = 200$ μm and $q_{\mathrm{CHF}} = 245$ kW m^{-2} for the plain surface (without porous particles) have been obtained. Note that the maximum q_{CHF} is increased by 3.33 times that of the plain surface using the coating modulation (when comparing sample 302 and the plain surface in [5]). According to the Zuber hydrodynamic stability theory, q_{CHF} is inversely proportional to the modulation wavelength which is assumed to be the channel pitch of the specimens [5]. As the modulation wavelength is reduced, further enhancement of q_{CHF} is expected. q_{CHF} for specimens 143, 147, 150, 302 and 313 vary from 611 kW m^{-2} to 815 kW m^{-2}. Although surface 302 reaches maximum q_{CHF}, it is regarded as experimental uncertainty due to the lack of geometric repeatability. The wick superheat of specimen 150 is the smallest that is desirable, i.e. reducing the wick superheat allows for lower temperature operation of the heat source. Figure 8 also indicates that q_{CHF} is nearly independent of the particle diameter of the porous coating, from the results 143, 150, 302 and 313.

It is possible that the Zuber theory is questionable, and detailed discussion of this theory (combining the Kelvin–

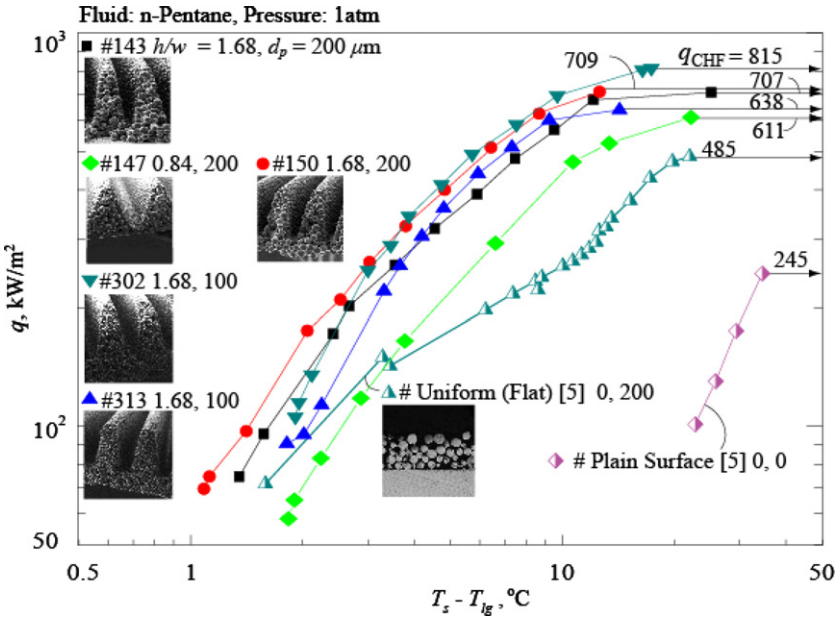

Figure 8. Variation of measured q_{CHF} with respect to surface superheat, for various coatings. The results for uniform coating and plain surfaces are also included for comparison purposes [5].

Helmholtz and Rayleigh–Taylor instabilities) and modulation of the single dominating wavelength are given in [5]. In [5, 19] a comparison of plain and modulated porous coating results shows that for the plain surface the Zuber prediction works fine and the modulated surface performance is also well predicted with this theory when the modulation wavelength is used. Also note that since there is no nucleate boiling when porous coatings with particles of the order of 100 μm in diameter are used, evaporation is from thin liquid films over particles (this is the reason for the smaller surface superheat compared to the plain surfaces where nucleate boiling occurs). Whether we used the columns where the liquid flows downward or the valleys where vapor flows upward, this modulated (created by surface structure) wavelength is the same.

Using optical and electron microscopy, it was found that the second method of fabrication resulted in closed surface pores. This would not allow for the penetration of liquid into the stacks (columns), so we cannot take advantage of the capillary liquid flow in the coatings and therefore did not test these samples. This capillary liquid flow is essential in supplying liquid to the base of the stacks for evaporation. When the liquid is not delivered to the base of the stack, the thermal resistance (which translates into surface superheat) becomes large since the heat has to flow a larger distance to reach the evaporation sites (this is explained and modeled in [5]). So, although the second method is drastically simpler to execute, it currently suffers from this surface pore closure and we need to explore means to open these pores (moderate acid treatment may achieve this). There is a slight fin (extended surface) advantage even with the closed surface pores, but compared to the first method, which utilizes the capillary flow in the stacks, this effect is small and not the focus here.

5. Conclusions

This study was aimed at determining the proper process conditions to manufacture microscale porous surface layers with modulations (i.e. channels) to be used in advanced heat transfer applications where volume, size and weight constraints are present. As a conclusion, it is found that it is feasible to produce microscale, porous and modulated surface layers bonded to a solid substrate using the warm compaction process. However, subsequent sintering has to be performed to maintain high bonding among powders with a substrate.

It was inferred from the porosity analyses that to achieve an acceptable range of porosity, it is adequate to keep temperature at low levels (∼350 °C) provided that enough bonding among the powders with a substrate is achieved before sintering. Based on the preliminary tests, it was observed that bonding capability between compacted powders and a substrate reduced when the tests were conducted below 350 °C and especially with low compaction pressures. To compensate the adverse effects of the low temperature on bond quality, high pressures are needed which result in lower porosity levels, which is another undesired feature of the surface intended. The low temperature conditions enable savings in manufacturing and handling time, energy, cost and equipment complexity. They would also reduce, if not eliminate, the oxidation problems during the mass manufacturing conditions.

In terms of manufacturability issues, the samples obtained with the first method (warm compaction and then sintering) have better formability and smaller valley thickness as required for improved heat transfer purposes compared to the second method results (sintering and then compaction). Moreover, stronger bonding between powders and a substrate was experienced in samples manufactured with the first method. In addition, the first method resulted in fewer ejection problems since lower pressures were applied. Although the second

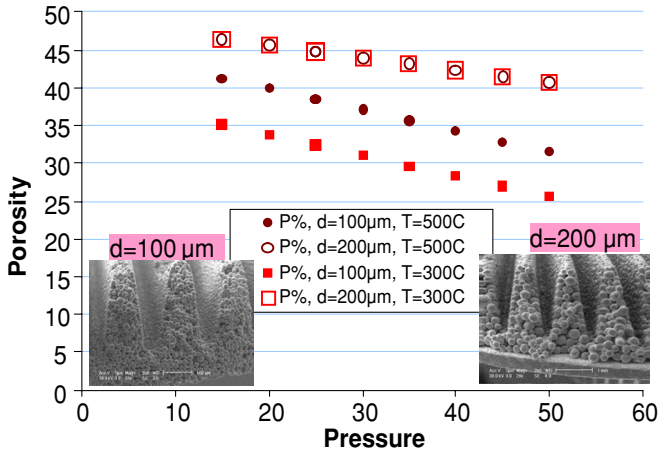

Figure 9. Comparison of porosity percentages at different temperature, pressure and powder levels.

method provides higher porosity in general, interconnectivity of the pores was not at the desired level in addition to the fact that the sidewalls of the channels were closed defeating the original purpose of porous modulations.

Another important observation was that the porosity did not change significantly when the aspect ratios (AR) of 0.84 and 1.68 were compared. High AR significantly contributed to the observed high CHF values. This observation indicates that the high AR does not lead to any disadvantages except a few practical difficulties during manufacturing such as ejection of compacted specimens out of die and insufficient filling of powders into the die cavity.

When response surface models for porosity from this study with 100 μm powders and a previous one with 200 μm powders [18, 19] are compared in figure 9 for an AR of 1.68, it becomes quite apparent that modulated surfaces with 100 μm powders result in ∼6–10% less porosity but still perform comparably, if not better, in CHF experiments as shown in figure 8.

Acknowledgments

The authors thank the National Science Foundation (NSF) for the partial support on this project through NSF ENG/CMMI grant 0638522. They also acknowledge the technical and financial support of Luvata Company for providing the technical support and specially designed roll mill for future studies.

References

[1] Reay D A 2002 Compact heat exchangers, enhancement and heat pumps *Int. J. Refrig.* **25** 460–70

[2] Boomsma K, Poulikakos D and Zwick F 2003 Metal foams as compact high performance heat exchangers *Mech. Mater.* **35** 1161–76

[3] Nishikawa K, Ito N and Tanaka K 1979 Enhanced heat transfer by nucleate boiling on a sintered metal layer *Heat Transfer Japan. Res.* **8** 65–81

[4] Chien L H and Chang C C Experimental study of evaporation resistance on porous surfaces in flat heat pipes *8th Intersociety Conf. on Thermal and Thermomechanical Phenomena in Electronic Systems, ITHERM 2002 (San Diego, CA, 29 May–1 June 2002)*

[5] Liter S G and Kaviany M 2001 Pool-boiling CHF enhancement by modulated porous-layer coating: theory and experiment *Int. J. Heat Mass Transfer* **44** 4287–311

[6] Webb R L 1983 Nucleate boiling on porous coated surfaces *Heat Transfer Eng.* **4** 71–82

[7] Hwang G-S and Kaviany M 2006 Critical heat flux in thin, uniform particle coatings *Int. J. Heat Mass Transfer* **49** 844–9

[8] Hwang G-S, Kaviany M, Anderson W G and Zuo J 2007 Modulated wick heat pipe *Int. J. Heat Mass Transfer* **50** 1420–34

[9] Min D H, Hwang G S and Kaviany M 2009 Multi-artery, heat-pipe spreader *Int. J. Heat Mass Transfer* **52** 629–35

[10] Chen Y M, Wu S C and Chu C I 2001 Thermal performance of sintered miniature heat pipes *Heat Mass Transfer* **37** 611–6

[11] Terpstra R L, Anderson I E and Gleeson B 2001 Development of metallic hot gas filters *Advances in Powder Metallurgy and Particulate Materials* (Princeton, NJ: MPIF-APMI) pp 1520–33

[12] Albano-Mueller L 1982 Filter elements of highly porous sintered metals *Powder Metall. Int.* **14** 73–9

[13] Mamalis A G, Petrossian G L and Manolakos D E 2000 Limit design of porous sintered metal powder machine elements *J. Mater. Process. Technol.* **98** 335–42

[14] Xie S and Evans J R G 2004 High porosity copper foam *J. Mater. Sci.* **39** 5877–80

[15] Shin H C and Liu M 2004 Copper foam structures with highly porous nanostructured walls *Chem. Mater.* **16** 5460–4

[16] Ngai T L, Wang S L, Li Y Y, Zhou Z Y and Chen W P 2005 Warm compaction powder metallurgy of Cu *Trans. Nonferr. Met. Soc. China (Engl. Ed.)* **15** 77–81

[17] Koç M, Usta Y and Karakoç A 2008 Investigations on thermo-mechanical fabrication of micro-scale porous surface features *J. Power Sources* **179** 592–602

[18] Cora Ö N, Usta Y and Koç M 2009 Micro-manufacturing of micro-scale porous surface structures for enhanced heat transfer applications—an experimental process optimization study *J. Micromech. Microeng.* **19** 045011

[19] Min D H, Hwang G S, Usta Y, Cora O N, Koc M and Kaviany M 2009 2-D and 3-D modulated porous coatings for enhanced pool boiling *Int. J. Heat Mass Transfer* **52** 2607–13

[20] AcuPowder International LLC Web site Last Access Date: 12 January 2009 http://www.acupowder.com/pdf/scu_shot.pdf

[21] Minitab–Statistical software, Minitab Inc., USA Web site address Last Access Date: 12 January 2009 http://www.minitab.com